Vehicle System Dynamics
Vol. 50, No. 10, October 2012, 1539–1562

Taylor & Francis
Taylor & Francis Group

Bifurcation analysis of an automobile model negotiating a curve

Fabio Della Rossa[a], Giampiero Mastinu[b]* and Carlo Piccardi[a]

[a]*Dipartimento di Elettronica e Informazione, Politecnico di Milano, via Ponzio, 34/5, Milano 20133, Italy;* [b]*Dipartimento di Meccanica, Politecnico di Milano, via La Masa, 34, Milano 20158, Italy*

(*Received 21 July 2011; final version received 20 March 2012*)

The paper deals with the bifurcation analysis of a rather simple model describing an automobile negotiating a curve. The mechanical model has two degrees of freedom and the related equations of motion contain the nonlinear tyre characteristics. Bifurcation analysis is adopted as the proper procedure for analysing steady-state cornering. Two independent parameters referring to running conditions, namely steering angle and speed, are varied. Ten different combinations of front and rear tyre characteristics (featuring understeer or oversteer automobiles) are considered for the bifurcation analysis. Many different dynamical behaviours of the model are obtained by slightly varying the parameters describing the tyre characteristics. Both simple and extremely complex bifurcations may occur. Homoclinic bifurcations, stable and unstable limit cycles (of considerable amplitude) are found, giving a sound and ultimate interpretation to some actual (rare but very dangerous) dynamic behaviours of automobiles, as reported by professional drivers. The presented results are cross-validated by exploiting handling diagram theory. The knowledge of the derived set of bifurcations is dramatically important to fully understand the actual vehicle yaw motions occurring while running on an even surface. Such a knowledge is a pre-requisite for robustly designing the chassis and for enhancing the active safety of vehicles.

Keywords: two-wheel model; tyre characteristics; handling diagram theory; two-parameter bifurcation analysis; active safety

1. Introduction

The great majority of drivers uses for most of the time their automobiles within the linear range of tyre characteristics [1]. In other words, a suitable mathematical model for describing the normal everyday running of an automobile can safely be linear. There are, however, rare but important cases in which the automobile exploits the nonlinear part of the tyre characteristics. A major example refers to accident avoidance manoeuvres, in which a well-designed vehicle can make the difference between a dramatic or an even unnoticed event. Motorsport is another field in which the tyre nonlinear characteristics play a crucial role. Usually, control laws for the anti-lock braking system and for the yaw motion are tested on iced surfaces to let

*Corresponding author. Email: gianpiero.mastinu@polimi.it, mastinu@mecc.polimi.it

ISSN 0042-3114 print/ISSN 1744-5159 online

http://dx.doi.org/10.1080/00423114.2012.679621
http://www.tandfonline.com

nonlinear phenomena occur in a repeatable way. The aim of this paper is to focus on the many different dynamic behaviours that are possible as a consequence of different combinations of the nonlinear characteristics of the tyres. As a matter of fact, a comprehensive understanding of such phenomena can enable a robust design of both the vehicle and its nonlinear controls devoted to enhance active safety.

A general approach for studying and classifying the behaviours of a nonlinear system when one or a few parameters are varied is *bifurcation analysis* [2]. In the recent literature on road vehicle dynamics [3,4], bifurcation analysis has been successfully applied to study driveline vibrations [5], vertical vibrations [6,7], tractor semi-trailer vibrations [5,8], and the interaction among vehicles in the traffic (vehicle following and overtaking) [9]. Nonlinear controls for enhancing stability have also been conceived based on bifurcation analysis [10,11].

The nonlinear dynamic behaviour of an automobile was first addressed in a smart early contribution [12], later refined in the excellent book by Pacejka [8]. Other refinements were given in [13,14]. In [8] a bifurcation analysis was performed to assess qualitatively how automobiles miss their stability and which kind of transient motion has to be expected when the equilibrium is disturbed. In [13], a further analysis with respect to what appeared in [12] was presented. In [14], the main problem addressed in the present paper was stated and shortly dealt with, and the complete spin of cars was studied. In [15–17], bifurcation analysis of the running vehicle were performed on rather complex vehicle systems in which the driver action is included.

In none of the above contributions, however, a comprehensive analysis has been made referring to all the possible behaviours that can be found by combining in every possible way the tyre nonlinear characteristics. This paper attempts to cover such a fundamental issue, in the perspective of modern bifurcation analysis. Bifurcation diagrams will be produced to analyse at a glance the influence on bifurcations of a couple of parameters.

A well-known problem – often underestimated or even neglected when analysing vehicle dynamics – is the computation of the equilibria of road vehicles at high lateral acceleration levels [3,4,8]. Usually only one equilibrium is computed, neglecting the existence of the many additional equilibria that are possibly generated by the nonlinear characteristics of tyres [3,4]. The *handling diagram* theory [8] is an invaluable tool to support the bifurcation analysis of the dynamic behaviour of a road vehicle and, for this reason, such a theory will be used hereafter. A detailed bifurcation analysis will be carried out on a relatively simple model of a car, allowing to perform a complete and reliable computation of the many occurring equilibria. Although based on a simplified model, the results presented in this paper are significant and important, because the simple two degrees-of-freedom (d.o.f.) model can reproduce the actual vehicle motion when the ground surface is slippery (e.g. with ice or snow). Indeed, in such a case, the forces acting on the suspension system are small and their influence on the motion of the vehicle is almost negligible, so that the suspensions can be removed from the model [1]. Actually, all the control systems for enhancing stability (such as Anti-lock Braking System and Electronic Stability Program) are often designed by means of the addressed two d.o.f. systems presented in this paper, the validation tests being performed on slippery surfaces [18].

The paper is organised as follows. First, we present the model used for the analysis. Then the bifurcations of equilibria are computed for a number of different combinations of front and rear tyre characteristics, and the results are verified and discussed by using the handling diagram theory. The cases of particular interest are highlighted. For the reader who is not familiar with bifurcation analysis, the basic theoretical tools used in the paper are described in the appendix. Similarly, a concise introduction to the handling diagram theory is given in Section 3 for those who are not familiar with this tool, although this part can be skipped without compromising the reading of the remainder.

2. System model

The mechanical model used for the bifurcation analysis is the well known two d.o.f. *single-track model* [1,8,13,19] shown in Figure 1. The main hypotheses are:

- the forward speed u is constant;
- the centre of gravity lies at the ground level;
- the vehicle body is modelled referring to its longitudinal axis;
- the resultant of the forces acting at the fore and rear axles are applied at the centres of the axles;
- the slip angles $\alpha_i, i = 1, 2$, and the steering angle δ (see Figure 1) are small;
- no longitudinal forces are acting at the wheels.

Under such hypotheses, the equations of motion read [8]

$$\begin{aligned} m(\dot{v} + ur) &= F_{y_1} + F_{y_2}, \\ I_z \dot{r} &= F_{y_1} a - F_{y_2} b, \end{aligned} \tag{1}$$

where v is the lateral speed, r is the yaw rate, subscripts 1 and 2 refer, respectively, to the front and rear axle, F_{y_i} is the lateral force on the ith axle, m is the vehicle mass, a and b are the horizontal distances, respectively, of the front and the rear axle centre from the vehicle's centre of mass, I_z is the moment of inertia of the vehicle around the vertical axis at the centre of gravity.

The kinematical variables are related by the following equations:

$$\begin{aligned} -\alpha_2 &= \frac{v - rb}{u}, \\ \delta - \alpha_1 &= \frac{v + ra}{u}. \end{aligned} \tag{2}$$

Eliminating v and r from Equations (1) and (2), it is possible to rewrite the equations of motion as the following ordinary differential equations:

$$\dot{\alpha} = f(\alpha, u, \delta) \Rightarrow \begin{cases} \dot{\alpha}_1 = \dfrac{g}{u}\left[(\delta - \alpha_1 + \alpha_2)\dfrac{u^2}{gl} - \dfrac{F_{y_1} + F_{y_2}}{mg} - \dfrac{a(F_{y_1} a - F_{y_2} b)}{I_z g}\right] \\ \dot{\alpha}_2 = \dfrac{g}{u}\left[(\delta - \alpha_1 + \alpha_2)\dfrac{u^2}{gl} - \dfrac{F_{y_1} + F_{y_2}}{mg} - \dfrac{b(F_{y_2} b - F_{y_1} a)}{I_z g}\right], \end{cases} \tag{3}$$

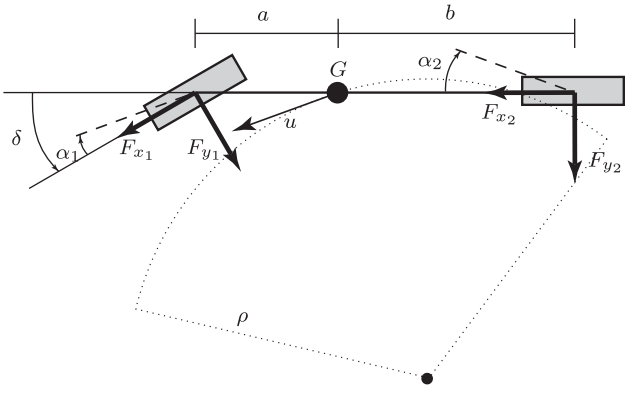

Figure 1. Representation of the *single-track model*.

Table 1. Parameter values of the vehicle model used in the paper.

Mass	m	950 kg
Moment of inertia around the vertical axis	I_z	1100 kg m^2
Wheelbase	l	2.46 m
Distance of the front axle centre from the centre of mass	a	0.95 m

where g is the gravitational acceleration and $l = a + b$ is the wheelbase. The lateral forces F_{y_i} $(i = 1, 2)$ can be expressed as functions of the slip angles α_i by the *tyre characteristics*, which are nonlinear and take the analytical form [8]

$$\begin{aligned} F_{y_1}(\alpha_1) &= D_1 \sin(C_1 \tan^{-1}(B_1\alpha_1 - E_1(B_1\alpha_1 - \tan^{-1}(B_1\alpha_1)))), \\ F_{y_2}(\alpha_2) &= D_2 \sin(C_2 \tan^{-1}(B_2\alpha_2 - E_2(B_2\alpha_2 - \tan^{-1}(B_2\alpha_2)))), \end{aligned} \tag{4}$$

where

$$D_1 = \mu_1 \frac{mg}{l} b, \quad D_2 = \mu_2 \frac{mg}{l} a,$$

and μ_1 and μ_2 are the friction coefficients, respectively, of the front and the rear tyres.

The parameter set can be divided into three subsets: the vehicle parameters (m, I_z, a, l), whose values are reported in Table 1, the tyre parameters $(\mu_i, B_i, C_i, E_i, i = 1, 2)$ which will be specified in the next section, and the parameters (u, δ) which represent the driver inputs.

3. Computation of the equilibria by the handling diagram theory

The behaviour at the steady-state cornering of the vehicle model of Figure 1 can be obtained by a geometrical procedure which is based on the *handling diagram* theory [8,13,19,20], an invaluable tool to analyse the nonlinear effects at high lateral acceleration levels. For the sake of brevity, only the basic elements will be summarised here – a detailed treatment can be found in [8] to which the reader is referred for a complete treatment. At steady state, after a proper arrangement of the equations of motion of the vehicle (referring both to lateral and vertical directions), the following relationships can be derived [8,20]:

$$\frac{F_{y_1}}{F_{z_1}} = \frac{F_{y_2}}{F_{z_2}} = \frac{u^2}{\rho g}, \tag{5}$$

where ρ is the radius of the negotiated curve, and F_{z_i} $(i = 1, 2)$ are the vertical forces acting, respectively, at the front and rear tips of the beam of Figure 1. The F_{z_i}-s are orthogonal with respect to the horizontal plane where the beam lies, and represent the resultants of the vertical forces acting, respectively, at the front and rear axles of the vehicle. Such resultants read as follows (see Figure 1):

$$F_{z_1} = mg\frac{b}{l} \quad F_{z_2} = mg\frac{a}{l}. \tag{6}$$

The key fact described by Equation (5) is that, at steady-state cornering, the values of *effective axle characteristics* F_{y_1}/F_{z_1}, F_{y_2}/F_{z_2} are given once the non-dimensional lateral acceleration $u^2/(\rho g)$ is specified.

Equation (5) can be geometrically interpreted as shown in Figure 2: on the right side of the figure, the effective front and rear axle characteristics $F_{y_1}(\alpha_1)/F_{z_1}$, $F_{y_2}(\alpha_2)/F_{z_2}$ are drawn as functions of the respective front and rear slip angles. Equation (5) implies that each horizontal

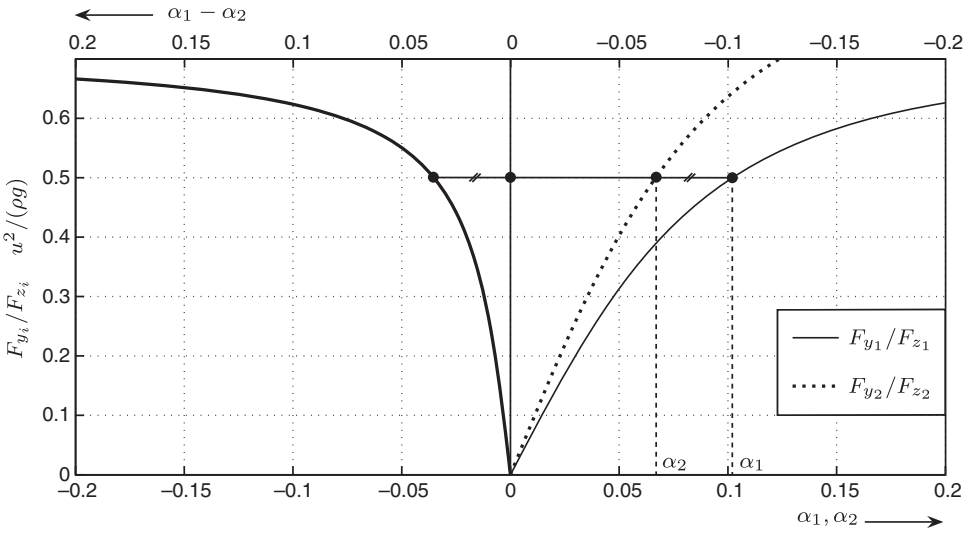

Figure 2. Representation of Equation (5) and construction of the handling curve. Right: front and rear effective axle characteristics (continuous line $F_{y_1}(\alpha_1)/F_{z_1}$, dotted line $F_{y_2}(\alpha_2)/F_{z_2}$). Left: derivation of the handling curve by taking the difference of the two effective axle characteristics at a given value of $u^2/(\rho g)$. Notice that the handling curve is a function of $\alpha_1 - \alpha_2$: the axis $\alpha_1 - \alpha_2$ is reported on top of the figure.

line (at a given $u^2/(\rho g)$) defines the lateral slips α_1 and α_2 at steady-state cornering. By taking the difference $\alpha_1 - \alpha_2$ at each given value $u^2/(\rho g)$, the *handling curve* in the left part of the figure is derived. The handling curve is a function of $\alpha_1 - \alpha_2$: the $\alpha_1 - \alpha_2$ axis is reported on the top of the figure.

As described in [1,8], the quantities $\delta, l, \rho, \alpha_1, \alpha_2$ are related by

$$\delta = \frac{l}{\rho} + \alpha_1 - \alpha_2, \tag{7}$$

so that the handling curve provides information on the steering angle δ needed to negotiate a curve of radius ρ. Consider now the diagram of Figure 3: on the left side, we replicate the handling curve plotted in Figure 2, whereas on the right side, which is the plane $(l/\rho, u^2/(\rho g))$, every straight line through the origin is a locus of points at equal constant speed, since $u^2/(\rho g) = \gamma(l/\rho)$ implies $\gamma = u^2/(gl) =$ constant. Given a vehicle model (specified by the wheelbase l and by the handling curve), the driver inputs (u, δ) univocally determine both the straight line with slope $\gamma = u^2/(gl)$, and its translation to the left of the quantity δ (see the dashed line in Figure 3), since $\delta = l/\rho + \alpha_1 - \alpha_2$. At this point, the intersection of the handling curve with the dashed straight line yields the values of $\alpha_1 - \alpha_2$ and $u^2/(\rho g)$ and, consequently, of the curve radius ρ. All the variables characterising the steady-state behaviour have, therefore, been obtained.

From what is illustrated above, it is evident that the handling curve is a fundamental tool for describing the vehicle behaviour. In Figures 4 and 5, a number of handling curves are plotted with the corresponding tyre parameters: they are obtained for different combinations of front and rear tyre characteristics. The handling curves are divided into two groups: vehicles that at low lateral acceleration $u^2/\rho g$ are understeering (labelled UN) in Figure 4, and vehicles that at low lateral acceleration are oversteering (labelled OV) in Figure 5. A vehicle is defined as understeering (resp. oversteering) if [1]

$$\frac{\partial(\delta - l/\rho)}{\partial(u^2/\rho g)} = \frac{\partial(\alpha_1 - \alpha_2)}{\partial(u^2/\rho g)} < [>]0. \tag{8}$$

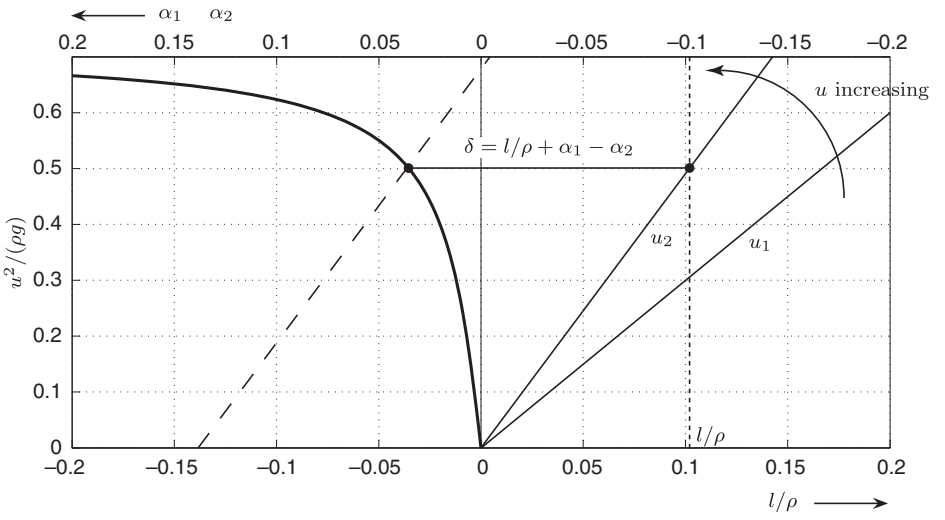

Figure 3. The steady-state behaviour of a car negotiating a curve at speed u with steering angle δ is obtained by translating the straight line with slope $u^2/(gl)$ to the left of a quantity δ, and finding the intersection with the handling curve.

In other words, the understeering (resp. oversteering) character is related to the negative (resp. positive) derivative of $\alpha_1 - \alpha_2$ with respect to $u^2/(\rho g)$ in the handling curve. Physically, this means that, increasing the speed, an understeering (resp. oversteering) vehicle naturally increases (resp. decreases) the radius of the bend which is negotiating.

It is important to notice that, since the handling curve is derived as the difference $\alpha_1 - \alpha_2$ at a given $u^2/(\rho g)$, depending on the functional form of the front and rear effective axle characteristics multiple equilibria can be obtained, especially at high lateral acceleration levels. For example, in the case of Figure 6(a), multiple equilibria are found if we fix the speed u and vary the steering angle δ. Indeed, three different equilibria are found at $\delta = \delta^A = 0$ and at $\delta = \delta^B \neq 0$, two at $\delta = \delta^C$, and only one at $\delta = \delta^D$. In Figure 6(b), the different steady-state attitudes of the vehicle model of Figure 1 at the different equilibria pointed out in Figure 6(a) are shown.

4. Bifurcation analysis

A general approach for studying Equation (3) is provided by *bifurcation analysis*, which is a powerful tool of nonlinear systems theory aimed at analysing and classifying the behaviours of a system when one or more parameters are varied [2]. Typically, the analysis starts by studying an equilibrium, and by deriving the dependence of its coordinates on a parameter. In doing so, a *bifurcation*, namely a structural change in the system behaviour, is possibly detected. By systematically analysing all the equilibria and their bifurcations, a complete catalogue of the system behaviours with respect to the admissible parameters' values is eventually derived. A concise review of the main concepts of bifurcation analysis is in the appendix, where the reader will find a description of all the terms used in this section.

A detailed, introductory example is presented in Figure 7, where the same case as that of Figure 6 is considered. The upper-left panel displays the dependence of the equilibria coordinates (α_1, α_2) on the parameter δ. The curves are obtained by means of a *continuation algorithm*. As already pointed out in the previous section, for small values of the steering

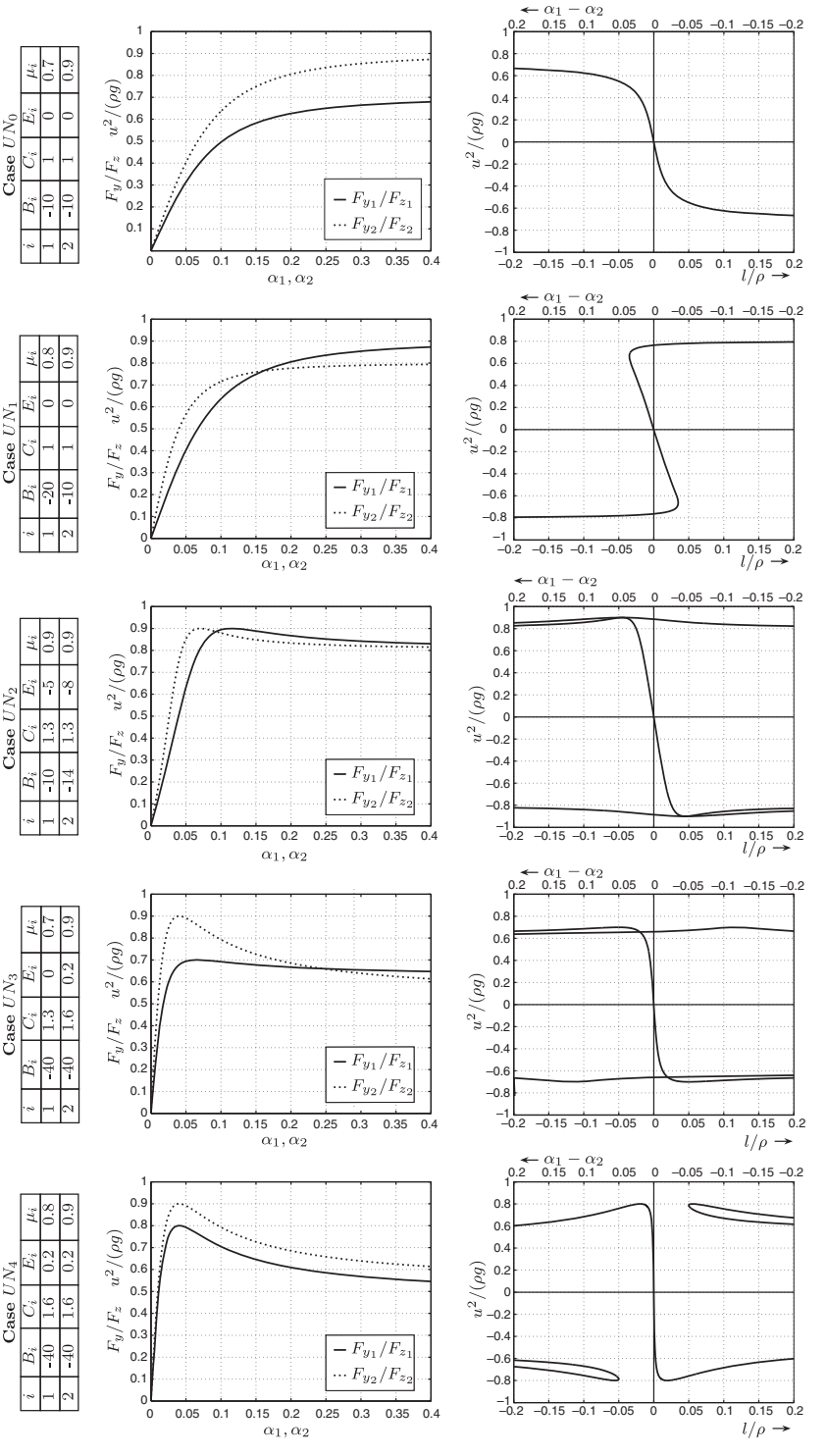

i	B_i	C_i	E_i	μ_i
1	-10	1	0	0.7
2	-10	1	0	0.9

i	B_i	C_i	E_i	μ_i
1	-20	1	0	0.8
2	-10	1	0	0.9

i	B_i	C_i	E_i	μ_i
1	-10	1.3	-5	0.9
2	-14	1.3	-8	0.9

i	B_i	C_i	E_i	μ_i
1	-40	1.3	0	0.7
2	-40	1.6	0.2	0.9

i	B_i	C_i	E_i	μ_i
1	-40	1.6	0.2	0.8
2	-40	1.6	0.2	0.9

Figure 4. Different types of understeering vehicles at low lateral acceleration. In the left column, the coefficients of the tyre characteristics (Equation (4)) are reported. In the central column, the effective axle characteristics are plotted (continuous line $F_{y_1}(\alpha_1)/F_{z_1}$, dotted line $F_{y_2}(\alpha_2)/F_{z_2}$). In the right column, the corresponding handling diagrams are derived. Notice that the plots in the right column are derived also for negative F_{y_i}, although not shown in the plots of the central column.

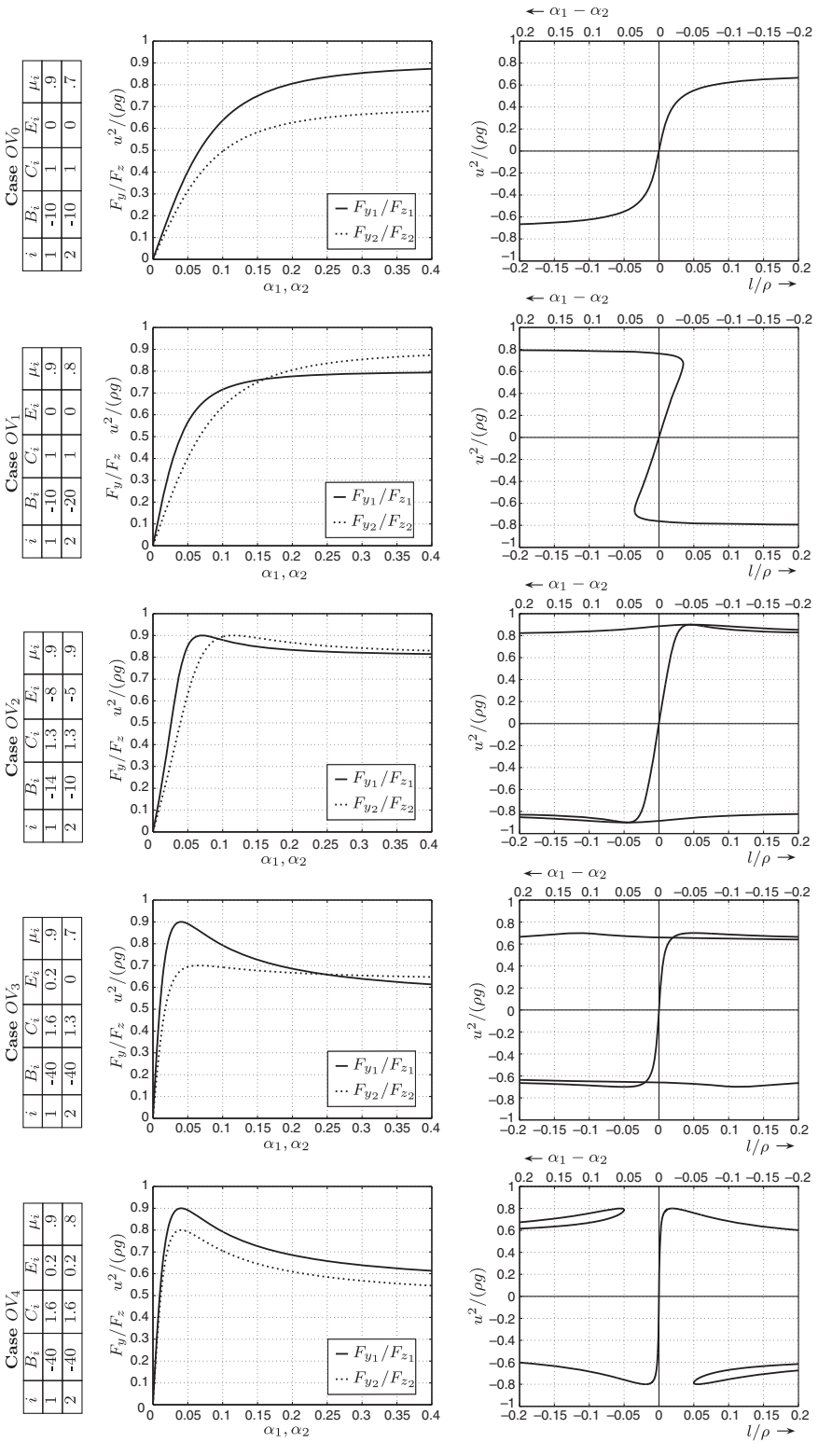

Figure 5. Different types of oversteering vehicles at low lateral acceleration.

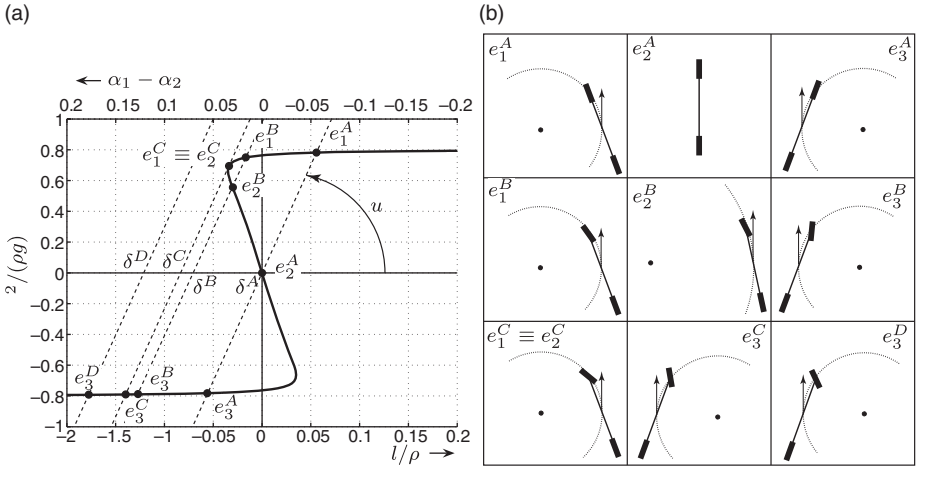

Figure 6. (a) Multiple equilibria of the vehicle model of Figure 1 are found from the handling curve, for a given speed u, at different steering angles δ^i $(i = A, B, C, D)$. (b) Steady-state attitudes of the vehicle of Figure 1 at the equilibria e_j^i $(j = 1, 2, 3)$.

angle ($\delta < \delta^C$), three equilibria are possible, denoted by e_j^i $(i = A, B, j = 1, 2, 3)$ in the figure. For a large steering angle ($\delta > \delta^C$), however, only one unstable equilibrium e_3^D exists. If we increase δ from 0, at $\delta = \delta^C = 0.0755$, the equilibria e_1 and e_2 collide and disappear in a *saddle-node* (*SN*) *bifurcation*, marking an abrupt qualitative change in the behaviour of the nonlinear system. The crucial role of the bifurcation also emerges from the phase plots Ⓐ to Ⓓ of Figure 7, which clearly show that the SN bifurcation divides the entire region of possible

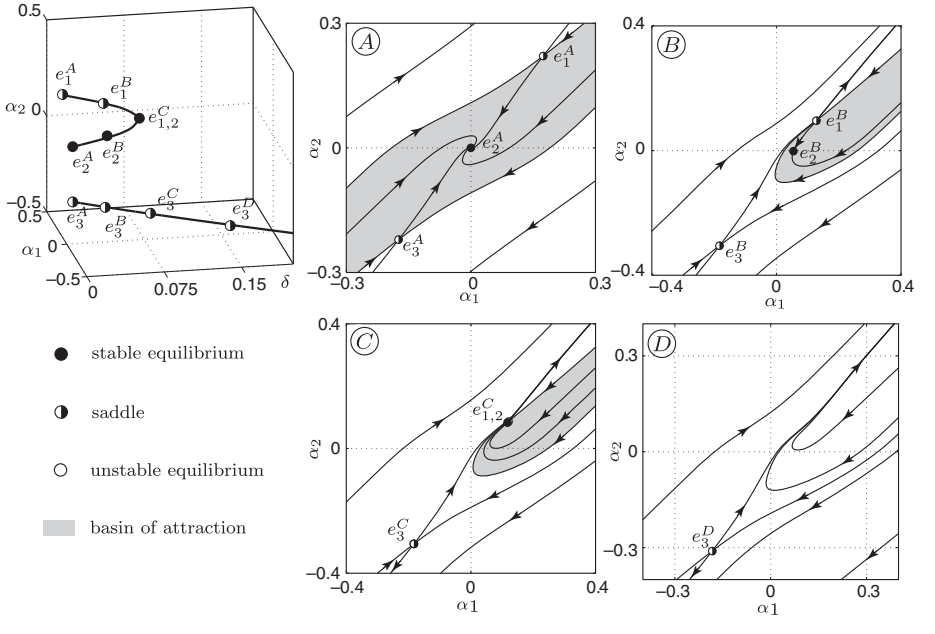

Figure 7. An example of bifurcation analysis of the vehicle model of Figure 1 (Equation (3)) with respect to the parameter δ (the speed is fixed at $u = 20$). The phase portraits (right panels) correspond to the δ values marked from Ⓐ to Ⓓ in the bifurcation diagram (upper-left panel). No stable equilibria exist for $\delta > \delta^C$ (phase portrait Ⓓ).

running conditions into two well distinct parts, since only for $\delta < \delta^C$ a stable equilibrium exists.

Let us now compare the results of Figure 7 with those obtainable from the handling diagram theory. If we consider again Figure 6, for a given speed u and steering angle $\delta = \delta^A = 0$, we identify three different equilibrium behaviours, one stable and the other two unstable. By increasing δ, equilibria e_1 and e_2 approach each other and, at δ^C, they collide and disappear. This is exactly what has been observed by bifurcation analysis: however, even in this basic example, there is one phenomenon that only the latter approach is able to detect. Compare the phase planes Ⓐ and Ⓑ in Figure 7: an important, qualitative change takes place between them, since the basin of attraction of e_2 (the only stable equilibrium) changes its topology and dramatically shrinks: this greatly restricts the set of perturbations that can safely be absorbed. The phenomenon is due to a *heteroclinic bifurcation* occurring at a value of δ between δ^A and δ^B ($\delta = 0.072$), a type of bifurcation that can be detected and studied with standard tools.

Since bifurcations play a strategic role for understanding the vehicle dynamics, we will focus on finding the combinations of the input parameters (δ, u) at which system (3) has a bifurcation. These combinations define the *bifurcation curves* in the (δ, u)-plane, which separate regions with different qualitative behaviours. Consider, for example, the problem of deriving the SN bifurcation curve. We already have one point of this curve, because the analysis of Figure 7 revealed, for fixed $u = 20$, an SN bifurcation at $\delta = 0.0755$. By a proper continuation algorithm (see Appendix), the entire SN curve in the (δ, u) can be derived. A similar approach can be followed for obtaining the heteroclinic (HET) bifurcation curve. The results are depicted in the left panel of Figure 8. Any combination (δ, u) on the left of the SN curve refers to cases in which a stable equilibrium exist, whereas no stable equilibria are found on the right of SN. Moreover, by crossing the HET curve from the left to the right, the basin of attraction of the stable equilibrium shrinks dramatically and changes topology (Figure 7).

It is worth noticing that, in principle, the SN curve can be obtained by means of the handling diagram too, as illustrated in the right panel of Figure 8. In fact, the SN curve is the (δ, u) locus of points at which the dashed line is tangent to the handling curve. As the speed u increases, the slope of the tangent line increases too, but its intersection with the horizontal axis (i.e. the steering angle δ) decreases. When $u \to \infty$, the tangent line approaches the vertical

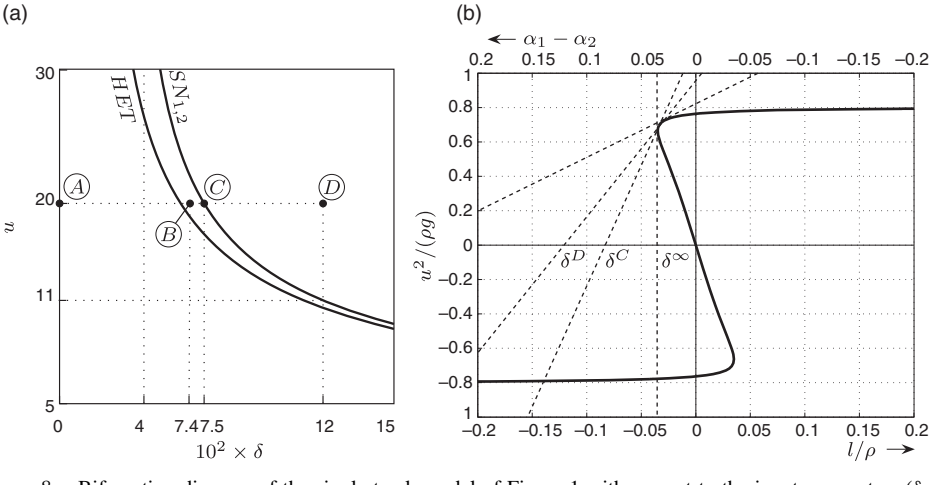

Figure 8. Bifurcation diagram of the single-track model of Figure 1 with respect to the input parameters (δ, u). Case UN_1 of Figure 4. $SN_{1,2}$ is a curve of SN bifurcation of equilibria e_1 and e_2, HET is a curve of heteroclinic bifurcation of the saddles e_1 and e_3. Points Ⓐ to Ⓓ correspond to the phase planes of Figure 7.

orientation and $\delta \to \delta^{\infty}$. For $\delta < \delta^{\infty}$ whatever speed u can be attained at stable steady-state running condition. Notice, however, that the handling diagram approach is unable to detect the phenomena connected with the heteroclinic bifurcation.

To summarise, we can claim that bifurcation analysis generalises the handling diagram approach and considerably enlarges its scope. As a matter of fact, in the remainder of this section, we will exhaustively analyse the 10 cases listed in Figures 4 and 5, and we will discover a variety of bifurcations which are associated with a variety of phenomena, from the sudden disappearance of stable equilibria (or of part of their basin of attraction, as in Figure 7), to the birth of oscillatory behaviours (limit cycles). Some of these phenomena can by no means be discovered by using handling diagrams. Furthermore, the approach of bifurcation analysis can in principle be applied to any model other than Equation (3), thus allowing a more refined description of the vehicle dynamic behaviour.

4.1. *Understeering cases*

4.1.1. *Case UN_0*

This case is extremely important because it corresponds to what should be obtained by a proper design of the automobile. Actually, only one stable equilibrium exists for every combination of the steering angle δ and forward speed u. It is a globally stable equilibrium, namely in principle any perturbation is absorbed, which implies that the vehicle is controlled by the driver in a relatively easy way. This case was discussed in [8].

The other cases, analysed below, basically take place as a consequence of a wrong design of the tyre-chassis system, or due to special occurrences such as unequal wear or irregular pressure of the tyres, for example.

4.1.2. *Case UN_1*

This case has already been considered before (Figures 6 and 7). Three equilibria occur (two unstable and one stable) and the basin of attraction suddenly shrinks as the forward speed u increases, as discussed in [13]. Two bifurcations take place: the first one is heteroclinic and its occurrence dramatically modifies the basin of attraction. The second bifurcation is an SN one, and can also be detected by inspection of the handling diagram, as shown in Figure 6(a).

4.1.3. *Case UN_2*

Three bifurcations occur in this case (which was partially analysed in [21]): heteroclinic, homoclinic, and Bogdanov–Takens. The first and second ones are briefly described in the appendix, whereas we refer to [2, p. 316], for details on the third one, although the basic phenomena related to this bifurcation are described below. The combined action of the homoclinic and Bogdanov–Takens bifurcations gives rise to an unstable limit cycle around the stable equilibrium, which limits its basin of attraction. Let us analyse the phase portraits of Figure 9:

- Ⓐ This is the most desirable situation for this case, although the basin of attraction is such that only bounded perturbations can be absorbed.
- Ⓑ Heteroclinic bifurcation. The unstable manifold of the SN e_3 is connected to the other saddle point e_1 instead of being connected to the stable equilibrium, as in the previous

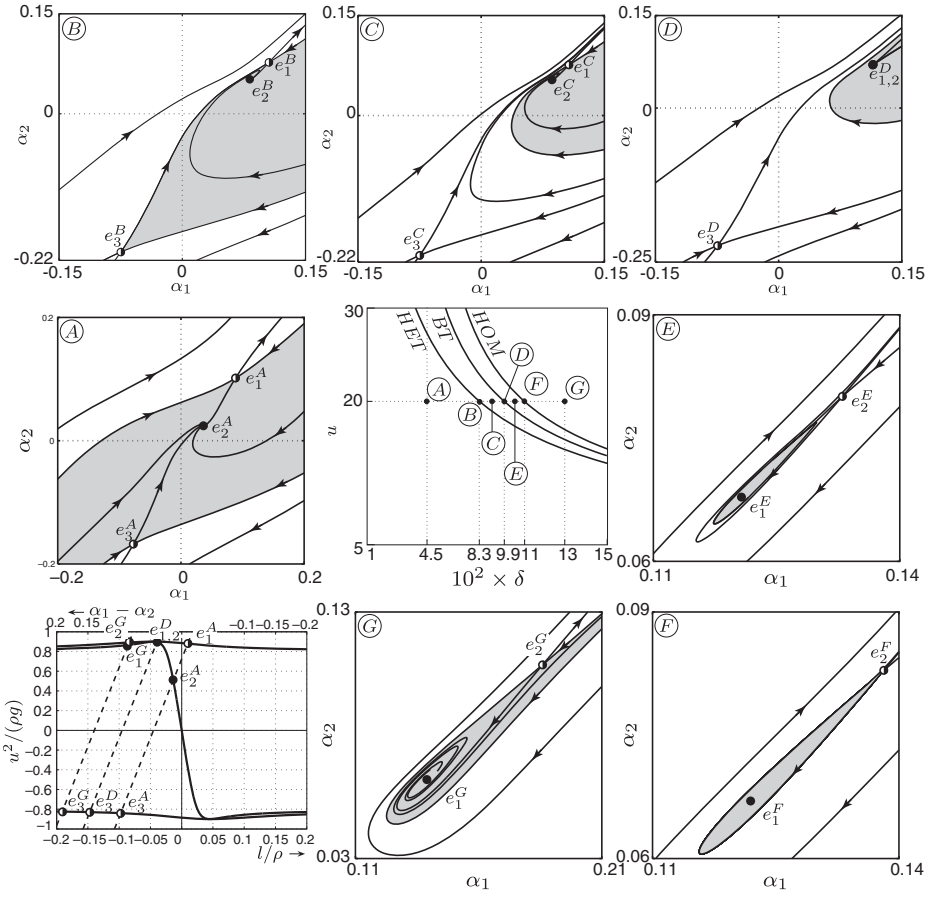

Figure 9. Bifurcation diagram of the single-track model of Figure 1 with respect to the input parameters (δ, u). Case UN_2 of Figure 4. The phase portraits Ⓐ to Ⓖ correspond to the (δ, u) values reported in the bifurcation diagram (central panel). *BT* is a curve of Bogdanov–Takens bifurcation.

case Ⓐ. The stable equilibrium is dangerously close to the border of the basin of attraction.

Ⓒ The basin of attraction is further shrunk, and is now defined by the stable manifolds of the saddle e_1 only. Again the stable equilibrium is almost on the border of its basin of attraction.

Ⓓ Bogdanov–Takens bifurcation: it is a complex bifurcation that occurs in this system because, due to symmetries, a number of phenomena take place at the same parameters' value. The equilibria e_1 (saddle) and e_2 (stable focus) merge but do not disappear. This is due to the fact that the axle characteristics have the same maximum value, as shown in the handling diagram of Figure 9. As a matter of fact, due to this simmetry a transcritical bifurcation takes place, instead of an SN one. An additional bifurcation (subcritical Hopf) actually occurs at this point, giving birth to an unstable limit cycle.

Ⓔ After the Bogdanov–Takens bifurcation, equilibria e_1 and e_2 have somehow exchanged their role, both topologically (now e_1 lies at the left of e_2) and dynamically (e_1 is now a stable focus and no longer a saddle). The basin of attraction around e_1 is now bounded by an unstable limit cycle, in accordance to what pointed out in [21]. The time period of the cycle varies between zero and infinity. Actually, just after the Bogdanov–Takens bifurcation the limit cycle is tiny and has small period. When the subsequent homoclinic

bifurcation is about to occur, the period of the limit cycle approaches infinity (see state portrait Ⓕ).

Ⓕ Homoclinic bifurcation. The stable and unstable manifolds of the saddle e_2 join each other. The limit cycle has disappeared.

Ⓒ The size of the basin of attraction, which is again unbounded on one side, increases with δ. The portrait is not much different than the one depicted in Ⓒ.

4.1.4. *Case UN$_3$*

The only bifurcation taking place in this case is a heteroclinic one (Figure 10).

Ⓐ Similarly to case UN$_1$, three equilibria can be found: one is a stable node, the others are saddles. The basin of attraction is bounded by the stable manifolds of the two saddles e_1 and e_3.

Ⓑ The basin of attraction is reduced and is now bounded by the stable manifolds of e_1 only.

In the previous cases UN$_1$ and UN$_2$, a relationship between bifurcations and handling diagram was pointed out, in the sense that we were able to infer some information about the occurrence of bifurcations by the exam of the handling diagram, especially at the intersections of its main branch with some isolated branches (see [8, p. 42]). This is not true in this case UN$_3$, because such intersections do not correspond to any bifurcation. As a matter of fact, in UN$_1$ and UN$_2$ the SN and Bodanov–Takens bifurcations occurred when the two equilibria e_1 and e_2 merged, i.e. when $(\alpha_1, \alpha_2)|_{e_1} = (\alpha_1, \alpha_2)|_{e_2}$. This obviously implies $(\alpha_1 - \alpha_2)|_{e_1} = (\alpha_1 - \alpha_2)|_{e_2}$, but the reverse is not true. Indeed, in case UN$_3$ we have that, when the latter equation holds (i.e. at the branch intersections of the handling diagram), the two equilibria remain distinct, namely $(\alpha_1, \alpha_2)|_{e_1} \neq (\alpha_1, \alpha_2)|_{e_2}$, so that no bifurcation occurs.

4.1.5. *Case UN$_4$*

In this case, two SN bifurcations occur (Figure 11). In the bifurcation diagram, the notation SN$_{i,j}$ refers to the collision of equilibria e_i and e_j.

Ⓐ For small values of the steering angle δ and of the speed u, five equilibria are present. The two couples of equilibria coming from the isolated branches of the handling diagram are all unstable (e_2 and e_4 are saddles, e_1 and e_5 are unstable nodes or foci), while the central equilibrium e_3 is stable. One of the branches of the stable manifold of the saddles

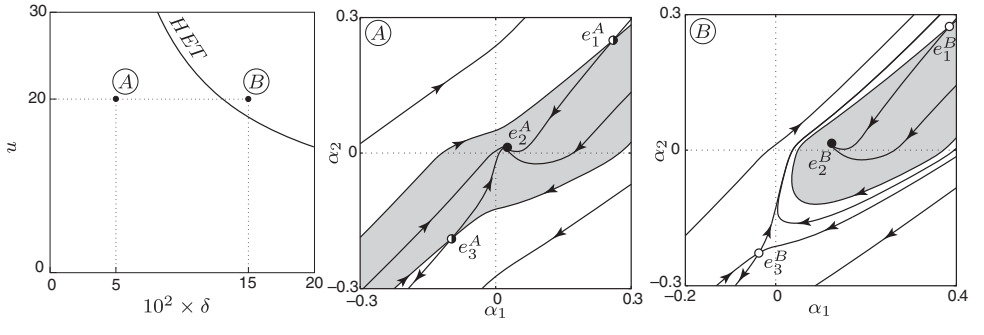

Figure 10. Bifurcation diagram of the single-track model of Figure 1 with respect to the input parameters (δ, u). Case UN$_3$ of Figure 4. The phase portraits Ⓐ and Ⓑ correspond to the (δ, u) values reported in the bifurcation diagram (left panel).

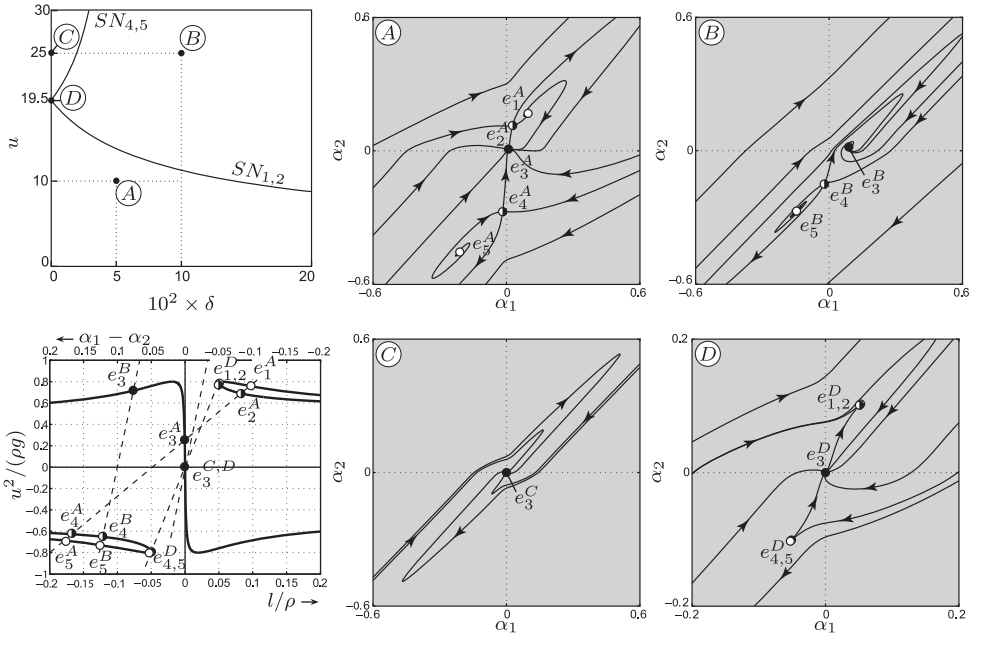

Figure 11. Bifurcation diagram of the single-track model of Figure 1 with respect to the input parameters (δ, u). Case UN_4 of Figure 4. The phase portraits Ⓐ to Ⓓ correspond to the (δ, u) values reported in the bifurcation diagram (upper-left panel).

is unbounded (i.e. it comes from infinity). The effect of this topology is the following: although trajectories converge to the stable equilibrium e_3 from any initial condition (with the exception of the four unstable equilibrium points), some trajectories will make a large tour before reaching e_3. This means that perturbations are absorbed but possibly with large overshooting.

Ⓑ At bifurcation $SN_{1,2}$ the saddle e_2 and the unstable equilibrium e_1 collide and disappear. The behaviour of the system does not change very much with respect to the previous case.

Ⓒ At bifurcation $SN_{4,5}$ the saddle e_4 and the unstable equilibrium e_5 collide and disappear.

Ⓓ This is a critical case in which two bifurcations simultaneously occur at the same parameter combination (δ, u).

4.2. *Oversteering cases*

4.2.1. *Case OV*$_0$

Three equilibria are possible for suitable (δ, u) values: two of them are saddles (e_1 and e_3) and the other is a stable node (e_2) (Figure 12).

Ⓐ, Ⓒ The stable manifolds of the saddles e_1 and e_3 form the boundary of the basin of attraction of the stable node e_2. Case Ⓐ represents a more dangerous situation than case Ⓒ because the stable equilibrium e_2^A is next to the border of the basin of attraction.

Ⓑ, Ⓓ The saddle e_1 and the stable equilibrium e_2 collide and disappear in an SN bifurcation $SN_{1,2}$. No stable behaviour is possible for (δ, u) values above the bifurcation curve.

At zero steering angle δ, if the forward speed u is increased, a different bifurcation occurs between Ⓒ and Ⓓ. It is a subcritical pitchfork bifurcation, in which the two saddles e_1 and e_3

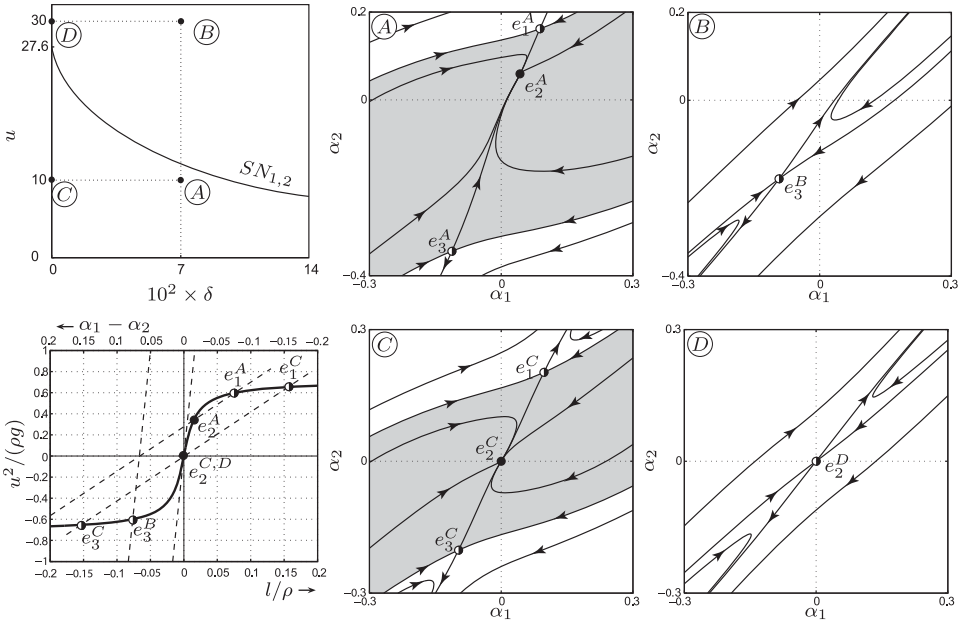

Figure 12. Bifurcation diagram of the single-track model of Figure 1 with respect to the input parameters (δ, u). Case OV_0 of Figure 5. The phase portraits Ⓐ to Ⓓ correspond to the (δ, u) values reported in the bifurcation diagram (upper-left panel).

collide with the stable equilibrium e_2, disappear and leave e_2, unstable, as the only equilibrium. This is the well-known unstable straight running of oversteering vehicles [8].

4.2.2. *Case OV*$_1$

Three SN bifurcations are found (Figure 13). Most notably, multiple stable equilibria are present, unlike the previous cases, which implies that, surprisingly, it is possible to negotiate different bends (up to three) at given speed and steering angle. The handling diagram reveals that the vehicle is actually oversteering at low lateral acceleration level, but understeering at high lateral acceleration levels. This implies that stable equilibria with high lateral acceleration can exist. It may even happen that the vehicle is unstable for straight running, but is stable at high lateral acceleration.

- Ⓐ Five equilibria are found: two of them are saddles (e_2, e_4) and three (e_1, e_3, e_5) are stable ones. The three basins of attraction cover the entire phase space, which implies that no perturbation gives rise to unstable behaviour. The stable manifolds of the saddles form the boundaries of the basin of attraction.
- Ⓑ The saddle e_2 and the stable equilibrium e_3 collide and disappear at the SN bifurcation $SN_{2,3}$. The bifurcation is catastrophic, but trajectories do not diverge to infinity, but remain bounded because they are captured by the basin of attraction of one of the other stable equilibria.
- Ⓒ Only one stable equilibrium is present. Surprisingly, if the steering angle δ is sufficiently large, increasing the forward speed u does not cause any catastrophe. Indeed, for $\delta \geq 4.3$, the equilibrium $e_{1,3}$ does not undergo any bifurcation (although its basin of attraction is modified).

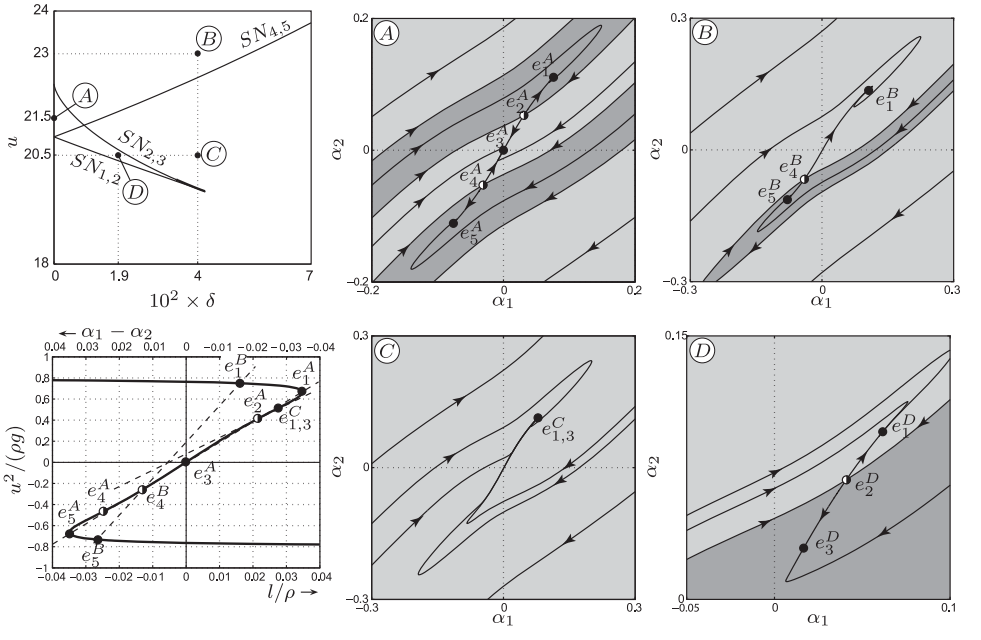

Figure 13. Bifurcation diagram of the single-track model of Figure 1 with respect to the input parameters (δ, u). Case OV_1 of Figure 5. The phase portraits Ⓐ to Ⓓ correspond to the (δ, u) values reported in the bifurcation diagram (upper-left panel).

Ⓓ Two stable equilibria exist, both with positive coordinates (α_1, α_2): they correspond to bends in the same direction but with different radii.

In order to better understand what happens in this case, let us consider the scenario in which at $u = u^D = u^C = 20.5$ the steering angle is increased from $\delta = 0$ to $\delta = \delta^C = 4$ (see the upper-left panel of Figure 13). At $\delta = 0$, e_3 is the only equilibrium and it is globally stable. Increasing δ, two more equilibria appear (e_1, e_2) when the bifurcation curve $S_{1,2}$ is crossed, but the driver does not feel anything because e_3 is unaffected by the bifurcation, although its global stability is lost. If δ is further increased, when the bifurcation curve $SN_{2,3}$ is crossed, the equilibrium e_3 suddenly disappears, giving rise to a rapid transient with the car negotiating a tighter bend.

4.2.3. *Case OV*$_2$

In this case, a stable limit cycle is found for suitable (δ, u) combinations. The parameter region in which such a limit cycle exists is bounded by a supercritical Hopf bifurcation curve (H) and a homoclinic bifurcation curve. Additionally, an SN bifurcation is present (Figure 14).

Ⓐ Five equilibria are present: four of them are unstable (e_1 and e_5 are foci, e_2 and e_4 are saddles) and one is stable (e_3). Actually, the only stable equilibrium is globally stable, i.e. any perturbation is absorbed.

Ⓑ The homoclinic bifurcation gives birth to a stable limit cycle, whose basin of attraction is delimited by the two branches of the stable manifold of the saddle e_2. Notice that this bifurcation cannot be predicted by inspection of the handling diagram.

Ⓒ At the $SN_{2,3}$ bifurcation, the stable equilibrium e_3 collides with the saddle e_2 and disappears. The only possible stable behaviour is now oscillatory, namely the stable limit cycle.

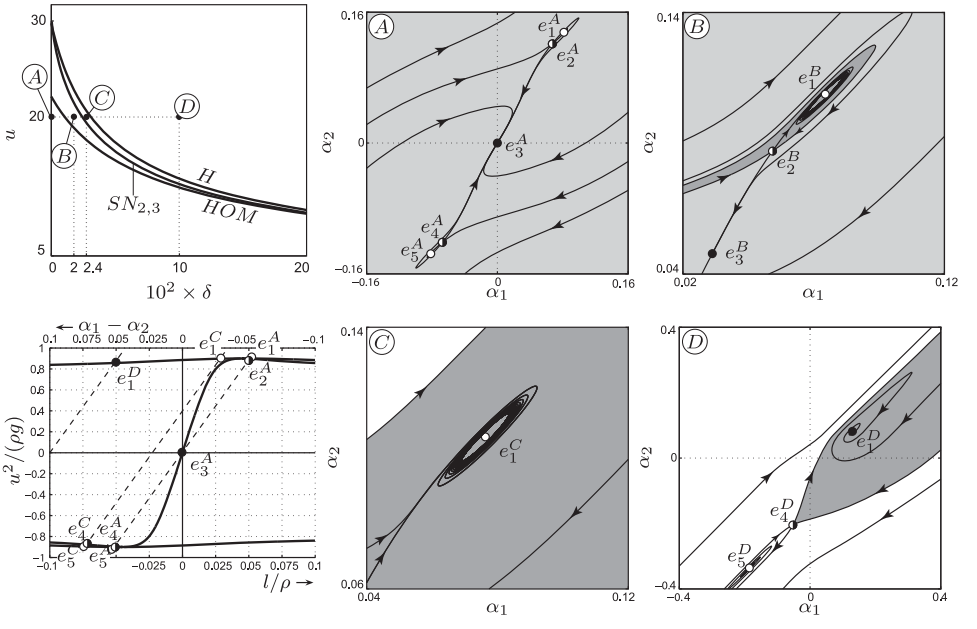

Figure 14. Bifurcation diagram of the single-track model of Figure 1 with respect to the input parameters (δ, u). Case OV_2 of Figure 5. The phase portraits Ⓐ to Ⓓ correspond to the (δ, u) values reported in the bifurcation diagram (upper-left panel).

The amplitude of the oscillation is considerable, being equal to 0.034 rad = 2°. This behaviour has been occasionally reported by professional drivers as a very dangerous situation.

Ⓓ The stable limit cycle disappears by shrinking on the unstable focus e_1 at the supercritical Hopf bifurcation. The cycle, which was born with infinite period at the homoclinic bifurcation, has now a period ranging from 2.55 to 2.65 s in the parameter window of Figure 14. Now e_1 becomes stable and its basin of attraction, which is the same of the former limit cycle, is bounded by the manifolds of the saddle e_4. Notice that in [8], some conditions for checking the local stability of an equilibrium from the handling diagram are reported. In principle, using those conditions, it is possible to reveal the Hopf bifurcation, but it is by no means possible to assess whether the limit cycle is stable.

4.2.4. *Case OV*$_3$

As for the previous case, a stable limit cycle of considerable amplitude exists for suitable (δ, u) combinations, namely in a region of the parameter plane which is bounded by an SN homoclinic (see [2, p. 250]) bifurcation curve ($SN_{2,3}$) and by a supercritical Hopf bifurcation curve (H) (Figure 15).

Ⓐ Five equilibria are present, four unstable (e_1 and e_5 are foci, e_2 and e_4 are saddles) and one globally stable (e_3). This phase portrait is topologically equivalent to the one labelled with Ⓐ in the OV_2 case.

Ⓑ At the SN homoclinic bifurcation $SN_{2,3}$, the saddle e_2 and the stable equilibrium e_3 collide. It must be pointed out that, in the phase portrait Ⓐ, both branches of the unstable manifold of e_2 terminate into the stable equilibrium e_3. As the bifurcation occurs, this generates a homoclinic loop and then a limit cycle which has initially finite amplitude and infinite

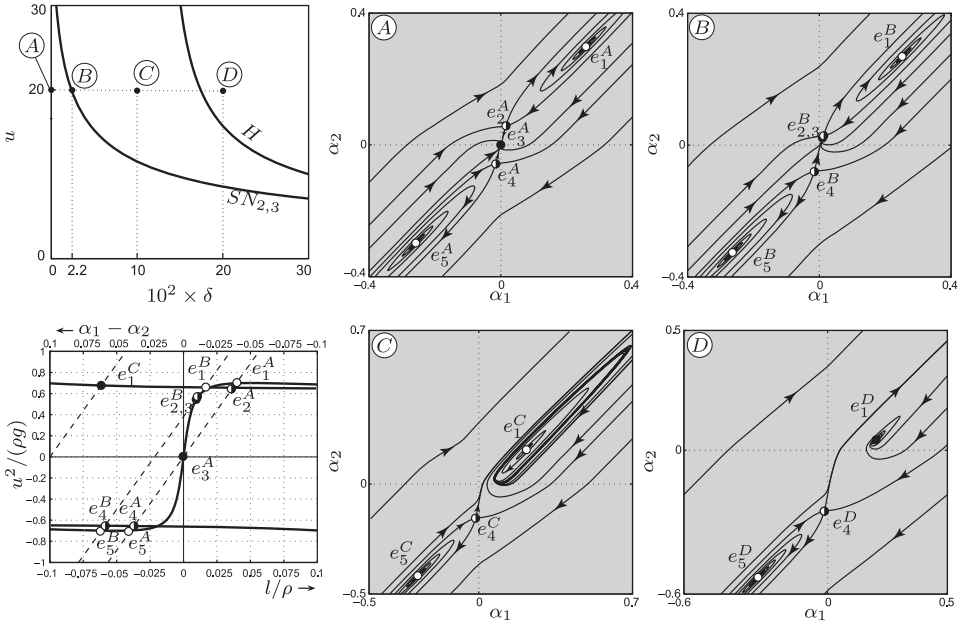

Figure 15. Bifurcation diagram of the single-track model of Figure 1 with respect to the input parameters (δ, u). Case OV_3 of Figure 5. The phase portraits Ⓐ to Ⓓ correspond to the (δ, u) values reported in the bifurcation diagram (upper-left panel).

period. We remark that this type of bifurcation cannot be predicted by inspection of the handling diagram.

Ⓒ After the $SN_{2,3}$ bifurcation, the only stable behaviour is oscillatory, namely a stable limit cycle. The amplitude of the limit cycle is very large (up to 0.6 rad) and decreases as δ is increased. Notice that this phase portrait is present in a wide region of the parameter plane.

Ⓓ The stable limit cycle shrinks on the unstable focus e_1 at a supercritical Hopf bifurcation, disappearing and changing the stability of e_1, which becomes now globally stable. On the Hopf curve, the cycle has a period ranging from 2.35 to 2.45 s.

4.2.5. *Case OV*$_4$

In this case,s we find two SN bifurcations, a homoclinic bifurcation, and a supercritical Hopf bifurcation (Figure 16). Again, a stable limit cycle of considerable amplitude is found.

Ⓐ If the speed u and the steering angle δ are small, three equilibria exist but only one of them is stable (e_4). The remaining two (e_3 and e_5) are saddles, and their stable manifolds form the boundary of the basin of attraction of e_4.

Ⓑ On the $SN_{3,4}$ bifurcation curve, the stable equilibrium e_4 collides with the saddle e_3 and disappears. After the bifurcation, no stable behaviour is present, namely all trajectories diverge and the vehicle is fully unstable.

Ⓒ If δ and/or u are increased, the isolated branches of the handling diagram generate (via SN bifurcation $SN_{1,2}$) two unstable equilibria, the saddle e_1 and the unstable focus e_2. One of the branches of the stable manifold of e_1 is connected to e_2. The vehicle is still fully unstable.

Ⓓ Crossing the homoclinic bifurcation, the stable and unstable manifolds of e_1 exchange their positions. A stable limit cycle is generated, with considerable amplitude (about

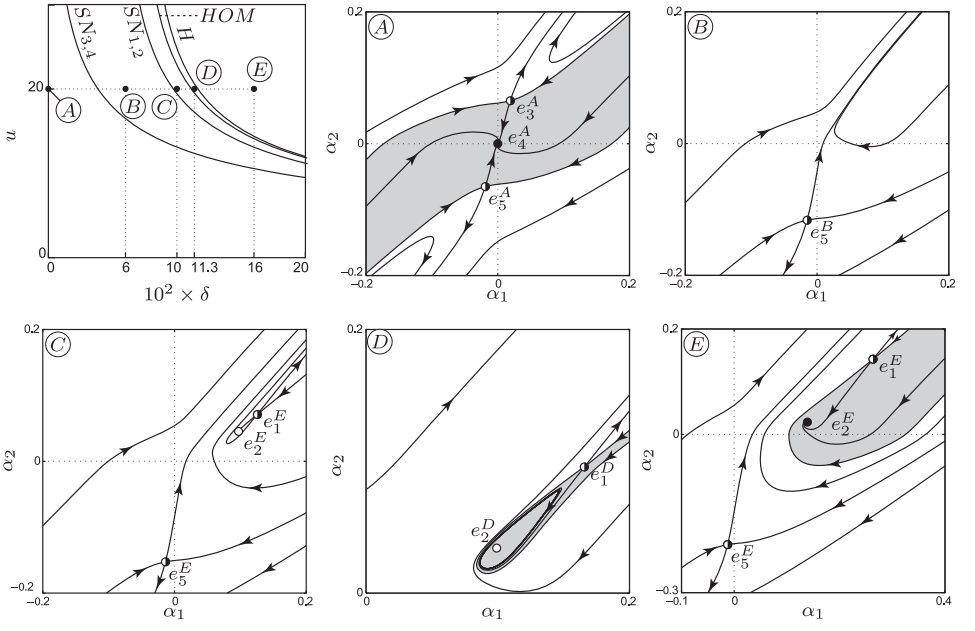

Figure 16. Bifurcation diagram of the single-track model of Figure 1 with respect to the input parameters (δ, u). Case OV_4 of Figure 5. The phase portraits Ⓐ to Ⓔ correspond to the (δ, u) values reported in the bifurcation diagram (upper-left panel).

0.1 rad = 6°). The limit cycle corresponds to the only stable behaviour, although its basin of attraction is rather small.

Ⓔ The limit cycle shrinks onto the unstable focus e_2, which thus becomes stable (supercritical Hopf bifurcation). Its basin of attraction (as in the previous panel Ⓓ) is bounded by the stable manifolds of the saddle e_1. On the Hopf curve, the disappearing cycle has a period ranging from 1.6 to 1.8 s.

5. Conclusions

The nonlinear dynamic behaviour of a vehicle cornering on even road surface has been studied. In particular, the bifurcation analysis of a two d.o.f. model has been performed to have an overview of its possible different dynamic behaviours. Ten different combinations of front and rear tyre characteristics have been considered, corresponding to five understeering and five oversteering vehicles. The bifurcation analysis has been conducted by varying two driver's input, namely the vehicle speed and the front wheel steering angle. A continuation technique has been employed to perform a two-parameter bifurcation analysis.

The results have been fully validated. Actually each phase portrait associated with a bifurcation plot has been analysed establishing a correspondence between the steady-state solutions computed in time domain by means of the nonlinear model and the corresponding steady-state solutions computed by means of the handling diagram theory.

An impressive variety of different possible dynamic behaviours appears by changing the nonlinear tyre characteristics even slightly. If the vehicle is always understeering, no bifurcations occur and unstable steady-state solutions never appear. This is a very good occurrence for active safety. If the vehicle is understeering at low centripetal acceleration levels only, or

isolated branches of the handling diagram are present, a number of quite different bifurcations may arise, depending on relatively small variations of the effective axle characteristics (i.e. tyre characteristics). Bifurcations occur if the forward speed is relatively high. Usually, increasing the steady-state steering angle decreases the speed at which the bifurcations occur. Heteroclinic, homoclinic, Saddle-Node, Bogdanov–Takens bifurcations have been reported. An unstable limit cycle has been also found.

The oversteering bifurcation cases are much more involved than the undesteering ones. The same considerations introduced for the undesteering vehicle hold. Heteroclinic, homoclinic, SN and Hopf bifurcations have been found and reported. Stable limit cycles have been also found. Extremely strange situations may occur, especially when multiple attractors are present. In this case, the vehicle can have different stable running conditions for the same driver's input.

The above results hold under the hypothesis of small values of both the lateral slips and the steering angle. A further investigation could be performed in the future removing such hypotheses and considering the full spin-out. No longitudinal forces at the tyres have been introduced and the body roll motion and the elastokinematics of the axles have been neglected. However, the different combinations of tyre characteristics taken into consideration provide – at least qualitatively – information on the effects of the neglected issues.

The handling diagram theory has been a useful source of information for bifurcation analysis. However, although some bifurcations can be detected by means of such a tool, only a partial understanding of the bifurcation scenario can be deduced by means of the handling diagram theory. Complex bifurcations, such as heteroclinic and homoclinc connections, and Hopf bifurcations remain undetectable by a simple inspection of the handling diagram.

The bifurcation analysis illustrated in the paper could be informative for chassis designers and control engineers who have to deal with the active safety of vehicles. In particular, it is confirmed that an understeering vehicle is to be always recommended. Besides, the original result coming from bifurcation analysis,is that the axle characteristics at the front and rear must be substantially different to obtain the widest possible attraction basin and ensure the maximum robustness of the design.

Acknowledgements

The authors would like to thank Vitaliano Nobile, who participated in a preliminary stage of the research.

References

[1] M. Mitschke and H. Wallentowitz, *Dynamik der Kraftfahrzeuge*, 4th ed., Springer, Berlin, 2004.
[2] A. Kuznetsov, *Elements of Applied Bifurcation Theory*, 3rd ed., Springer, New York, 2004.
[3] S. Bruni and G. Mastinu (eds.), *Proceedings of the 19th IAVSD Symposium: Dynamics of Vehicles on Roads and Tracks*, Milan, Italy, 2005.
[4] K. Hedrick (ed.), *Proceedings of the 20th IAVSD Symposium: Dynamics of Vehicles on Roads and Tracks*, Berkeley, CA, USA, 2007.
[5] R. Andrzejewski and J. Awrejcewicz, *Nonlinear Dynamics of a Wheeled Vehicle*, Springer, Berlin, 2005.
[6] L. Palkovics and P.J.T. Venhovens, *Investigation on stability and possible chaotic motions in the controlled wheel suspension system*, Veh. Syst. Dyn. 21 (1992), pp. 269–296.
[7] Q. Zhu and M. Ishitobi, *Chaos and bifurcations in a non linear vehicle model*, J. Sound Vib. 275 (2004), pp. 1136–1146.
[8] H.B. Pacejka, *Tire and Vehicle Dynamics*, 2nd ed., Elsevier, Oxford, 2006.
[9] G. Orosz, B. Krauskopf, and R.E. Wilson, *Bifurcations and multiple traffic jams in a vehicle-following model with reaction-time delay*, Physica D 211 (2005), pp. 277–293.
[10] B. Catino, S. Santini, and M. Di Bernardo, *MCS adaptive control of vehicle dynamics: An application of bifurcation techniques to control system design*, Proceedings of the 42nd IEEE Conference on Decision and Control, Maui, Hawaii, 2003, pp. 2252–2257.
[11] D.-C. Liaw and W.-C. Chung, *A feedback linearization design for the control of vehicle's lateral dynamics*, Nonlinear Dyn. 52(4) (2008), pp. 313–329.

[12] H.B. Pacejka, *Nonlinearities in road vehicle dynamics*, Veh. Syst. Dyn. 15(5) (1986), pp. 237–254.
[13] G. Mastinu and R. Cesarini, *Stability and drivability of vehicles in the horizontal plane (in Italian)*, ATA 44 (1991), pp. 430–442.
[14] P.A. Shavrin, *A chaotic dynamics of the vehicle on the plane*, Proceedings of the International Conference on Physics and Control, St. Petersburg, 2005, pp. 474–478.
[15] Z. Liu, G. Payre, and P. Bourassa, *Nonlinear oscillations and chaotic motions in a road vehicle system with driver steering control*, Nonlinear Dyn. 9 (1996), pp. 281–304.
[16] E. Ono, S. Hosoe, H.D. Tuan, and S. Doi, *Bifurcation in vehicle dynamics and robust front wheel steering control*, IEEE Trans. Control Syst. Technol. 6(3) (1998), pp. 412–420.
[17] H.Y. Hu and Z.Q. Wu, *Stability and Hopf bifurcation of four-wheel-steering vehicles involving driver's delay*, Nonlinear Dyn. 22 (2000), pp. 361–374.
[18] Arjeplog Test Center, Sweden. Available at http://www.arjeplogtestcenter.com/.
[19] H.B. Pacejka, *Simplified analysis of steady-state turning behaviour of motor vehicles*, Veh. Syst. Dyn. 21 (1973), pp. 269–296.
[20] Ja.M. Pevsner, *Theory of the stability of automobile motions*, Masjgiza Leningrad, St. Petersburg, Russia, 1947.
[21] S. Shen, J. Wang, P. Shi, and G. Premier, *Nonlinear dynamics and stability of vehicle plane motions*, Veh. Syst. Dyn. 45 (2007), pp. 15–35.
[22] J. Guckenheimer and P. Holmes, *Nonlinear Oscillations, Dynamical Systems, and Bifurcations of Vector Fields*, Springer, New York, 1983.
[23] A. Dhooge, W. Govaerts, and Yu. A. Kuznetsov, MATCONT: A MATLAB package fornumerical bifurcation analysis of ODEs, *ACM Trans. Math. Software* 29 (2002), pp. 141–164.

Appendix. Bifurcations in second-order continuous-time systems

In this appendix, which is oriented to readers not familiar with bifurcation analysis, we briefly review and describe the terms used in the paper. A detailed treatment of the topic can be found in standard textbooks, e.g. [2,22]. The model considered in the paper is a second-order, continuous-time, autonomous (i.e. time-invariant) system of the form

$$\begin{aligned} \dot{x}_1(t) &= f_1(x_1(t), x_2(t), p), \\ \dot{x}_2(t) &= f_2(x_1(t), x_2(t), p), \end{aligned} \tag{A1}$$

or $\dot{x}(t) = f(x(t), p)$ in vector notation. The two-dimensional vector $x(t) = [x_1(t) x_2(t)]$ is the state and $p = [p_1\ p_2\ \dots\ p_m]$ are the system parameters. For all possible initial states $x(0)$, we assume that the solution $x(t)$ of system (A1) is univocally defined for all $t \geq 0$. The oriented curve obtained by projecting a solution $x(t)$ onto the plane (x_1, x_2) is a *trajectory*. The set of the trajectories obtained for all possible $x(0)$ is the *phase portrait*.

For a given p, an equilibrium of system (A1) is a state $\bar{x}$ such that $\dot{x} = f(\bar{x}, p) = 0$. In most situations, the stability of $\bar{x}$ can be discussed through *linearisation*, namely by analysing the stability of the linear system $\dot{v}(t) = J(\bar{x}, p)v(t)$, where

$$J(\bar{x}, p) = \left[\frac{\partial f(x,p)}{\partial x}\right]_{x=\bar{x}} = \begin{bmatrix} \dfrac{\partial f_1(x,p)}{\partial x_1} & \dfrac{\partial f_1(x,p)}{\partial x_2} \\ \dfrac{\partial f_2(x,p)}{\partial x_1} & \dfrac{\partial f_2(x,p)}{\partial x_2} \end{bmatrix}_{x=\bar{x}}$$

is the Jacobian matrix at $x = \bar{x}$. The equilibrium $\bar{x}$ of system (A1) is *asymptotically stable* (or *stable* for brevity) when all trajectories starting sufficiently close to $\bar{x}$ remain close to it for all t, and converge to $\bar{x}$ as $t \to +\infty$. The *basin of attraction* $B(\bar{x})$ of a stable equilibrium is the set of all initial states from which the trajectories converge to $\bar{x}$, i.e.

$$B(\bar{x}) = \{x(0) | x(t) \longrightarrow \bar{x}\}.$$

A stable equilibrium $\bar{x}$ is *globally stable* when $B(\bar{x})$ is the entire phase plane (x_1, x_2), i.e. trajectories converge to $\bar{x}$ from any initial state $x(0)$ (with at most the exception of some isolated points and/or lines).

If we denote by λ_1, λ_2 the eigenvalues of $J(\bar{x}, p)$, then $\bar{x}$ is stable if $\mathrm{Re}(\lambda_i) < 0$ for $i = 1, 2$, namely if both the eigenvalues have a negative real part. On the contrary, if $\mathrm{Re}(\lambda_i) > 0$ for some i, i.e. if at least one eigenvalue has a positive real part, the equilibrium $\bar{x}$ is *unstable*, namely there are trajectories started arbitrarily close to $\bar{x}$ that diverge from it.

If we exclude non-generic situations (i.e. $\lambda_1 = \lambda_2$ or $\mathrm{Re}(\lambda_i) = 0$ for some i), the eigenvalues λ_1, λ_2 can be placed in the complex plane in five different qualitative positions only, to which five different phase portraits in the neighbourhood of $\bar{x}$ are associated. In these five cases, the equilibrium $\bar{x}$ is called, respectively, *stable/unstable focus*, *stable/unstable node*, or *saddle* (Figure A1). Note that stable (resp. unstable) foci/nodes are obviously stable (resp. unstable) equilibria, and that saddles are unstable too.

The *stable manifold* $W^S(\bar{x})$ is the set of initial states $x(0)$ such that $x(t) \to \bar{x}$ as $t \to +\infty$. Similarly, the *unstable manifold* $W^U(\bar{x})$ is the set of $x(0)$ such that $x(t) \to \bar{x}$ as $t \to -\infty$. All the states in the neighbourhood of a stable (resp. unstable) focus/node form its stable (resp. unstable) manifold. Instead, the stable (resp. unstable) manifold of a saddle is formed by the trajectories that converge to $\bar{x}$ in forward time (resp. backward time, i.e. by reversing the arrows on the trajectories) (see Figure A1(c)).

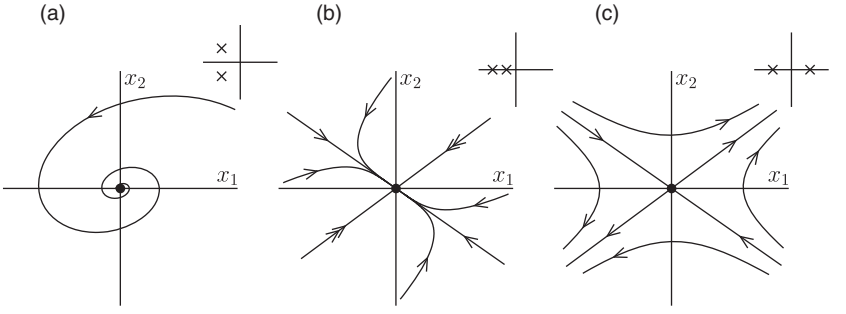

Figure A1. The phase portraits of the generic second-order systems in the neighbourhood of $\bar{x}$, with the corresponding position of λ_1, λ_2 in the complex plane: (a) *stable focus*; (b) *stable node* (the *unstable focus* and *unstable node* are obtained from (a) and (b), respectively, by reversing the arrows on the trajectories and by changing the sign of the real part of the eigenvalues); (c) *saddle*.

A key notion in bifurcation theory is that of *structural stability*. For a given parameter value $p = \bar{p}$, system $\dot{x} = f(x, \bar{p})$ is structurally stable if the phase portraits of all the systems $\dot{x} = f(x, p)$ with $|p - \bar{p}| < \varepsilon$ ($\varepsilon > 0$ arbitrarily small) are *topologically equivalent*, i.e. they can be obtained one from each other by continuous deformation. By contrast, by perturbing the parameter p of a *non*-structurally stable system, the behaviour of the system undergoes some structural change, e.g. an equilibria is born, or it disappears, or it switches from stable to unstable. A *bifurcation* is exactly such a qualitative change in the system behaviour that takes place when, by varying p, a value $p = p^*$ of non-structural stability is crossed. In the following, we list the types of bifurcations we found in analysing the model presented in the paper.

In an *SN bifurcation*, the system has two distinct equilibria on one side of the bifurcation (say, for $p < p^*$), one of them is a node and the other is a saddle. By varying p, the two equilibria collide (and coincide) at $p = p^*$ whereas, for $p > p^*$, no equilibria exist (Figure A2(a)). If the node existing for $p < p^*$ is stable, the bifurcation is *catastrophic*: if the system is in the stable state $\bar{x} = \bar{x}(p)$ for $p < p^*$, when p increases above the bifurcation value $p = p^*$ the stable node disappears and $x(t)$ jumps faraway towards, e.g. another stable equilibrium or periodic orbit (if it exists), or diverges to infinity. An SN bifurcation can be revealed by analysing the Jacobian evaluated at $\bar{x} = \bar{x}(p)$ since, when p is varied, $\det(J(\bar{x}(p), p))$ vanishes at the bifurcation point (i.e. one of the eigenvalues λ_1, λ_2 becomes zero).

A *transcritical bifurcation* is found when, by varying p, two distinct solution branches of the equilibrium equation $f(\bar{x}, p) = 0$ intersect and exchange their stability. In the typical scenario, the system has two equilibria on one side of the bifurcation ($p < p^*$), one of them stable and the other unstable. By varying p, the two equilibria collide at $p = p^*$ and then, for $p > p^*$, they become again distinct, but the stable branch has become unstable and vice versa (Figure A2(b)). Analytically, a transcritical bifurcation is characterised by $\det(J(\bar{x}(p), p)) = 0$ at $p = p^*$ (as for the SN bifurcation), plus suitable conditions on the higher-order derivatives of $f(x, p)$ [22, Ch. 3].

In a *pitchfork bifurcation*, the system has three distinct equilibria for $p < p^*$ and only one for $p > p^*$. The two most interesting scenarios are those of Figure A3. In the first one (*supercritical* pitchfork), two stable and one unstable equilibria collide leaving only one stable equilibrium. In the dual case (*subcritical* pitchfork), the bifurcation is catastrophic, since no stable equilibrium exists for $p > p^*$. As for the transcritical bifurcation, a pitchfork is characterised by $\det(J(\bar{x}(p), p)) = 0$ at $p = p^*$ plus suitable conditions on the higher-order derivatives of $f(x, p)$ [22, Ch. 3].

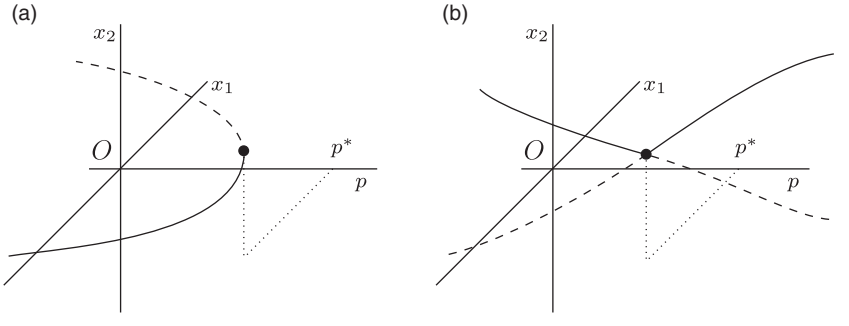

Figure A2. (a) Saddle-node and (b) transcritical bifurcations in second-order systems. Continuous (resp. dot) lines represent stable (resp. unstable) equilibria.

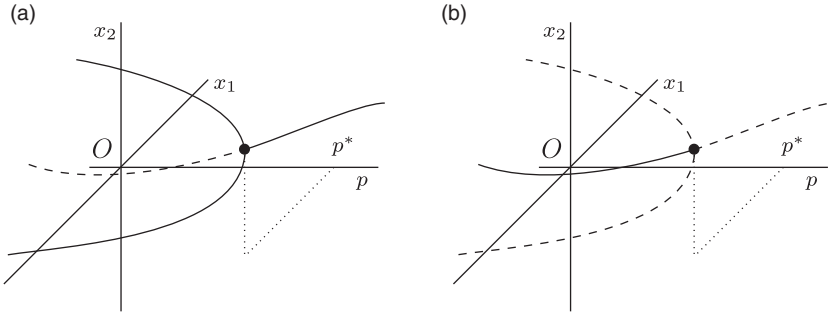

Figure A3. (a) Super- and (b) sub-critical pitchfork bifurcations in second-order systems.

A *Hopf bifurcation* is the transformation of a focus-type equilibrium into a limit cycle, i.e. a periodic, oscillatory solution of system (A1). In a *supercritical* Hopf bifurcation, the focus turns from stable to unstable at $p = p^*$ and, at the same time, a stable (i.e. attracting) limit cycle is born, initially with zero amplitude. Therefore, by increasing p from $p < p^*$, a stationary behaviour is smoothly replaced by an oscillatory one. In a *subcritical* Hopf bifurcation, instead, the limit cycle is unstable (i.e. it repels all neighbouring trajectories) and surrounds the stable equilibrium, actually delimiting its basin of attraction. In this case, the bifurcation is catastrophic (Figure A4). A Hopf bifurcation can be detected by analysing the eigenvalues $\lambda_{1,2} = a \pm i\omega$ of the Jacobian matrix of the focus, since the bifurcation corresponds to the change of sign of the real part a, i.e. $\lambda_{1,2} = \pm i\omega^*$ at $p = p^*$. The period τ of the emerging limit cycle is also related to $\lambda_{1,2}$, since $\tau \to 2\pi/\omega^*$ as $p \to p^*$.

A *homoclinic bifurcation* can be interpreted as the collision of a limit cycle with a saddle. A typical scenario is that of Figure A5: a stable limit cycle exists for $p < p^*$, containing an unstable focus at the inside. As $p \to p^*$, the cycle comes closer and closer to a saddle and, at the same time, its period $\tau \to \infty$. At $p = p^*$ the cycle is replaced by a *homoclinic loop*, formed by the stable and unstable manifolds of the saddle, which have joined. For $p > p^*$, the loop breaks and no stable equilibria nor cycles exist. Alternatively, we can interpret the bifurcation as a mechanism of birth of a limit cycle (for decreasing p) but, differently from the Hopf case, the emerging cycle has non-zero amplitude and an unbounded period. The dual situation (unstable limit cycle with stable focus) is also possible (not reported for brevity).

A *heteroclinic bifurcation* takes place at $p = p^*$ when the stable manifold of a saddle becomes coincident with the unstable manifold of another saddle. Crossing the value p^*, the behaviour in the vicinity of the saddles does not modify qualitatively, but a change takes place in the global structure of the phase portrait (Figure A6). This has typically an important impact on the basin of attraction of some neighbouring stable equilibrium.

An effective bifurcation analysis requires the use of suitable algorithms for numerically deriving the bifurcations curves. The most used algorithm is *continuation*, which is implemented in a number of software packages (in our study,s we used MATCONT [23]). Generally speaking, a continuation problem consists in finding a curve in a $(q + 1)$-dimensional space, when the curve is defined by a system of q equations $g(z, p) = 0$. Here, $z \in R^q$, p is scalar, and g is a q-dimensional vector function. If a point (z_0, p_0) of the curve is known, i.e. $g(z_0, p_0) = 0$, a predictor–corrector algorithm [2] can be used to find a sequence of points belonging to the curve.

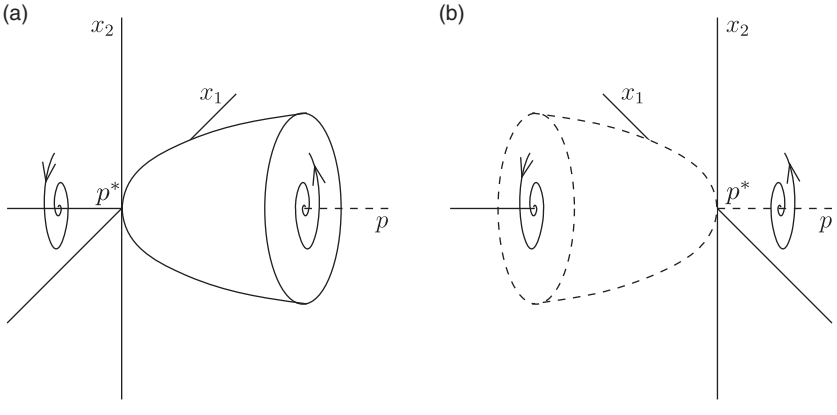

Figure A4. (a) Super- and (b) sub-critical Hopf bifurcations in second-order systems.

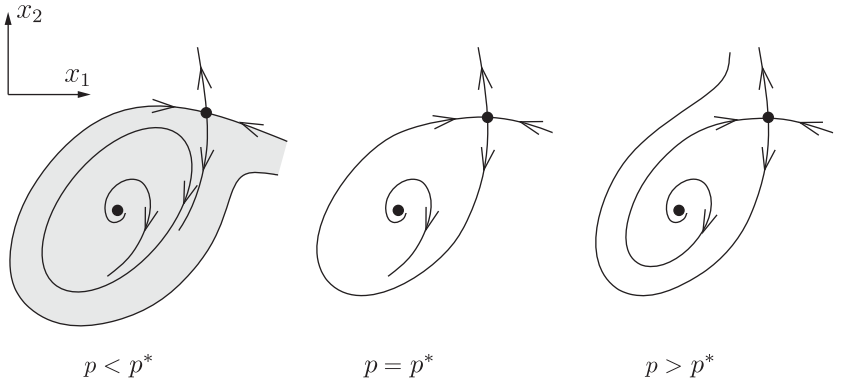

Figure A5. Homoclinic bifurcation in second-order systems.

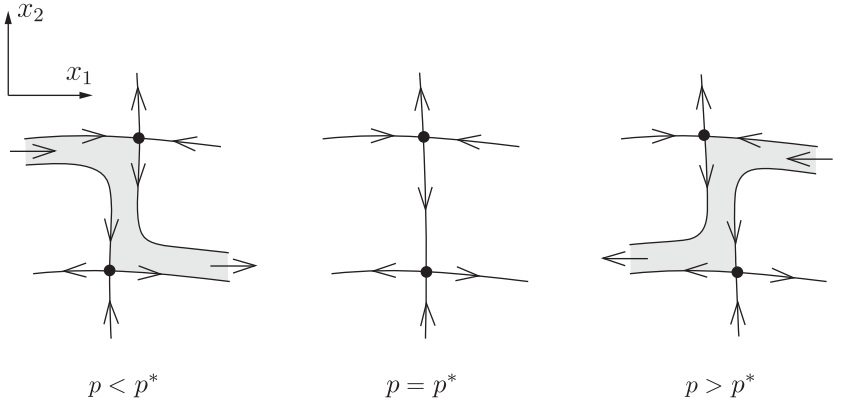

Figure A6. Heteroclinic bifurcation in second-order systems.

Every bifurcation curve can be obtained by solving a suitable continuation problem. For example, given the system $\dot{x} = f(x,p)$, the curve $\bar{x} = \bar{x}(p)$ describing the dependence of an equilibrium point $\bar{x}$ on a parameter p (Figure A2(a)) is simply defined by $f(x,p) = 0$. While obtaining this curve by point-by-point continuation, one can monitor a series of *bifurcation functions*, designed to change sign if a bifurcation occurs. For instance, as already pointed out above, $\det(J(\bar{x}(p),p)) = 0$ when an SN bifurcation occurs. Then, to derive the entire SN bifurcation curve in a two-parameter plane (p_1,p_2) (as shown in Section 4), the following continuation problem has to be solved:

$$f(x,p_1,p_2) = 0, \tag{A2}$$

$$\det(J(\bar{x}(p),p_1,p_2)) = 0. \tag{A3}$$

This system defines a curve in the four-dimensional space (x_1,x_2,p_1,p_2), whose projection onto the (p_1,p_2)-plane is the SN bifurcation curve. Similar procedures are used, upon defining a suitable bifurcation function, to analyse all types of bifurcations.